ELSEVIER

Solar Energy Materials & Solar Cells 76 (2003) 613–624

Solar Energy Materials & Solar Cells

www.elsevier.com/locate/solmat

Injection technique for the study of solar cell test structures

R. Ciach[a], Yu.P. Dotsenko[b], V.V. Naumov[c], A.N. Shmyryeva[d], P.S. Smertenko[b,*]

[a] *Polish Foundation for the Development of Material Sciences, Ul. Warszawska 24, 31-155 Krakow, Poland*
[b] *Department of Optoelectronics, Institute of Semiconductor Physics, National Academy of Sciences of Ukraine, Prospekt Nauki 45, 03028 Kyiv, Ukraine*
[c] *Institute of Fundamental Problems for High Technology, P.O. Box 58, 03028 Kyiv, Ukraine*
[d] *National Technical University of Ukraine-Kyiv Polytechnic Institute, Prospekt Peremogy 54, 04057 Kyiv, Ukraine*

Received 1 October 2001; received in revised form 18 February 2002

Abstract

Charge carrier injection and recombination processes in semiconductor solar cells is considered and analyzed. A differential approach based on an *I–V* characteristic approximation is introduced, in order to recognize the mechanisms of injection and recombination and to determine the physical parameters of photovoltaic semiconductor structures. Examples of application of the injection technique for investigation of typical silicon solar cell test structures are demonstrated.

Keywords: Solar cell; Charge injection; Test structure; *I–V* characterization

1. Introduction

Recombination of electrons and holes in a semiconductor material is one of the most important processes in photovoltaic (PV) solar cells that determines their physical and technical parameters. There are many techniques, based on optical, thermal, photo-activation and other phenomena, for investigation of recombination processes in PV semiconductors. An alternative approach for the determination of

*Corresponding author. fax: +380-44-265-8342.
E-mail address: eureka@irva.kiev.ua (P.S. Smertenko).

0927-0248/02/$ - see front matter
PII: S0927-0248(02)00271-4

the recombination peculiarities is a charge carrier injection method. Injection processes play a major role in the charge flow mechanism in the thin semiconductor layer, when its thickness L ranges between the Debye screening length and the diffusion length of the carriers. Injection and recombination mechanisms of both types of charge carrier affect the shape of the I–V characteristics. On the other hand, analysis of the I–V characteristics permits one to control the parameters of barrier semiconductor structures, monopolar and bipolar injection, hopping, ionic, percolation and other charge carrier mechanisms. The charge carrier injection, being another way of enhancement of the concentrations of both types of carrier in the semiconductor structure, allows one to determine such physical parameters as the minority carrier recombination lifetime, the surface recombination rate, the local density of states distribution in the forbidden bandgap, the electron or hole capture cross-sections for these local states, etc.

The purpose of this work is to demonstrate the features of our technique based on the charge carrier injection phenomena for the investigation of the electro-physical properties and the characterization of typical silicon solar cell test structures based on microcrystalline Si, SiC and porous Si.

2. Methodology

Charge carrier injection processes in semiconductors have been investigated worldwide during the years 1960–1980. The theoretical fundamentals of contact-injection phenomena, involving charge injection from the contacts into the solid-state, including wide-gap semiconductors, appropriate boundary conditions, charge density and recombination rate have been developed and applied. Examples of this abound [1–9].

The analysis of the mechanisms of both charge carriers injection and recombination sets an essential variety in the behavior of injected carriers and their influences on the current–voltage (I–V) characteristics. In the Table 1, we summarize our knowledge about basic approximations of the I–V characteristics of semiconductor structures that are available and applicable in solar cells, as well as providing a model classification of the regimes of injection and recombination that take place in the test cells depending upon the conditions of operation [2,3,8,10–15]. The basic physical characteristics of the test structures (concentrations of carriers, recombination rates, diffusion lengths, etc.) that can be determined from the respective I–V characteristics in each injection regime are also presented in the Table 1.

The distribution of the local density of states $S(E)$ is determined by, following [12–14,16]:

$$S(E) = -\frac{1}{2ekT} \times \frac{\mathrm{d}}{\mathrm{d}n_\mathrm{s}}\left[n_\mathrm{s}^4 \times \frac{\mathrm{d}^3\rho_\mathrm{S}}{\mathrm{d}n_\mathrm{s}^3}\right], \tag{13}$$

where $E = kT \times \ln 3N_\mathrm{C}/2n_\mathrm{s}$ is the energy from the bottom of the conduction band; $N_\mathrm{C} = 2(2\pi m^* kT/h^2)^{3/2}$ is the effective density of states near conduction

Table 1
Basic approximations of the current–voltage characteristics and regimes of injection and recombination processes in solar cell structures

Value α (1)	Approximation equation for the I–V dependence (2)	Formula number (3)	Regime of injection and recombination (4)	Reference (5)	Determined parameters (6)
$0<\alpha<1$ min	$j(V)=e\mu_n n_K\frac{V}{L}\frac{\exp\{\varepsilon e d_K V/\varepsilon_K kTL\}}{1+2\mu_n V/u_n D_K L}$	(1)	Regime of constant field between contacts	[10]	n_K; S_K; d_K
$\alpha=1$	$j(V)=e\mu_n n_o V/L$	(2)	Ohm's law	[2,9]	n_0
$\alpha=1$	$j(V)=e\mu_n n_K(V-V_K)/L$	(3)	Contact limited current	[8,11]	n_K; ρ_K/e
$0<\alpha<1.5$	$V(j)=[1-j/j_i]jL/\sigma$	(4)	Regime of low injection	[9]	ρ_K/e
$\alpha=1.5$	$j(V)=\frac{8}{9}e\left[\frac{2\mu_n\mu_p(\mu_n+\mu_p)}{\gamma_z}\right]^{0.5}\frac{V^{3/2}}{L^2}$	(5)	Double injection in semiconductor, bimolecular recombination	[2,3,9]	n_s; γ_z
$\alpha=2$	$j(V)=\frac{9}{8}\frac{\varepsilon\mu_n V^2}{L^3}$	(6)	Monopolar injection in a semiconductor or dielectric without traps	[2,9]	μ_n
$\alpha=2$	$j(V)=\frac{9}{8}\frac{\varepsilon\mu_n V^2}{\theta L^3}$	(7)	Monopolar injection in a semiconductor or dielectric with traps	[2,9]	μ_n/θ
$\alpha=2$	$j(V)=\frac{3}{4}\left[\frac{\pi\varepsilon\mu_n\mu_p(\mu_n+\mu_p)}{\gamma_z}\right]^{0.5}\frac{V^2}{L^3}$	(8)	Double injection in an ideal dielectric, bimolecular recombination	[2,3,9]	n_s; γ_z
$\alpha=2$	$j(V)=\frac{9}{8}e\mu_n\mu_P\left[\frac{(\gamma_n+\gamma_p)}{\gamma_n\gamma_p N_r}\right]\lvert\Delta N\rvert\frac{V^2}{L^3}$	(9)	Double injection in a semiconductor, monomolecular recombination	[2,3,9]	$n_s; r\frac{\gamma_n\gamma_P}{(\gamma_n+\gamma_P)}$

Table 1 (*continued*)

Value α (1)	Approximation equation for the I–V dependence (2)	Formula number (3)	Regime of injection and recombination (4)	Reference (5)	Determined parameters (6)
$\alpha > 2$ max	—	(10)	Traps field limited (monopolar injection) or recombination limited (double injection)	[2,3,9,12–14]	$S(E)$; $R(E)$; N_r; E_r; $\tau_{n,p}$
$\alpha = 3$	$j(V) = \frac{125}{72\pi} e\mu_n\mu_p\gamma_n \frac{V^3}{L^5}$	(11)	Double injection in an ideal dielectric, monomolecular recombination	[2,3,6,9]	n_s; τ_n
$\alpha = 4$	$j(V) = \frac{21609}{131072\pi^2} \frac{eh^6}{(\gamma_z E_g)^3} \left[\frac{\mu_n\mu_p(m_n+m_p)}{m_n m_p}\right]^{0.5} \frac{1}{(\mu_n+\mu_p)} \frac{V^4}{L^7}$	(12)	Super-high double injection	[15]	n_s; L_s; γ_z

V is the applied voltage; I is the through current; j, j_n and j_p are the full, electron and hole current densities; α is the differential slope of the $I-V$ characteristic; e is the electron charge; h is Planck's constant; ε is the dielectric constant of the semiconductor; ε_K is the contact energy gap; μ_n, μ_p are the mobilities of electrons and holes; E_g is the forbidden bandgap of the semiconductor; γ_z, γ_n, γ_p are the rate coefficients for zone–zone, electron and hole recombination; n_o, n_K, n_s are the concentrations of ohmic, contact and bulk current carriers; S_K is the surface recombination rate; d_K is the contact gap width; ρ_K/e is the charge density near the contact; L_s is the ambipolar diffusion length, τ_n, τ_p are the average lifetimes of electrons and holes; θ is the sticking coefficient.Table 1

Basic approximations of the current–voltage characteristics and regimes of injection and recombination processes in solar cell structures

band edge;

$$\rho_S = \frac{\xi}{4\pi L^2}\frac{d}{d(1/I)_l}\left[\frac{d(V/I^2)_l}{d(1/I)_l}\right]$$

is the density of space charge,

$$n_s = \frac{L}{e\mu S}\times\frac{d(1/I)_l}{d(V/I^2)_l}$$

is the density of free electrons; k is the Boltzmann's constants; m^* is the effective mass of the electron; and T is the absolute temperature.

In order to recognize the above mentioned regimes and mechanisms of injection and recombination in a test solar cell structure, a differential technique for processing experimental I–V characteristics can be introduced. This technique of differential analysis of the $y = f(x)$ dependence (where x is the argument, y is the function) implies the mathematical determination of dimensionless values in the form [9,17,18]:

$$\alpha(x) = \frac{d(\lg y)}{d(\lg x)} = \frac{x}{y}\frac{dy}{dx}, \tag{14}$$

$$y(x) = \frac{d(\lg \alpha)}{d(\lg x)} = \frac{x}{\alpha}\frac{d\alpha}{dx}, \tag{15}$$

Here, the first value characterizes a power-law dependence in form $y(x) = x^{\alpha}$, and the second one an exponential law in form $y(x) = \exp(x^{\gamma})$. While the processing of the $y(x)$ dependence uses formula (14), one will reveal regions with $\alpha(x) = \text{constant}$. These are the regions where the $y(x)$ dependence is adequately approximated by a power law. Similarly, while the treatment of the $y(x)$ dependence uses formula (15), one will find the regions with $\gamma(x) = \text{constant}$. These regions correspond to an almost exponential behaviour of $y(x)$. The accuracy of $\alpha(x)$ and $\gamma(x)$ determination is limited by the errors of measurements, Δ_x and Δ_y, respectively. If systematic errors due to the transition from the infinitesimal steps to the finite steps are taken into account, Δ_α and Δ_γ can be given by

$$\Delta_\alpha = 0.3[1/2a^2 - 11/2/\alpha]^{1/3}(\Delta_y + \alpha\,\Delta_x)^{2/3}, \tag{16}$$

$$\Delta_\gamma = 0.3[1/2\gamma^2 - 11/2/\gamma]^{1/3}(\Delta_\alpha + \gamma\Delta_x)^{2/3}. \tag{17}$$

The normal procedure for the test solar cell structure investigation is as follows:

(1) Experimental measurements of the steady-state I–V characteristic of the test sample in the dark and under illumination, under forward and reverse bias;
(2) Mathematical processing of the I–V curve by the differential technique;
(3) Analysis of the fine structure of the current in the I–V characteristic, and determination of the ranges of constancy and extremes ($\alpha_{min}, \alpha_{max}$) for the $\alpha - V$ dependence with respect to the voltage;
(4) Recognition of the main injection and recombination regimes, and determination of the basic physical parameters of the test structure by the injection approach.

Besides electro-physical characterization, further optimization of the test solar cell structure utilizing this approach is also possible [19].

3. Results of the investigations

We have conducted experimental studies for three types of solar cell test structure based on: (1) microcrystalline Si, (2) microcrystalline SiC, and (3) porous Si. For illustration, Fig. 1 shows the measured steady-state I–V characteristics of the test structures, and Fig. 2 presents the results of their differential treatment in the form of the $\alpha - V$ dependences.

Microcrystalline Si and SiC layers were obtained by standard PECVD technology. Si layers were obtained by deposition from SiH_4 gas in a RF discharge plasma (power 30–160 W) at a temperature of 500°C, and SiC layers were obtained by deposition of CH_3SiCl_3 gas in a RF discharge p

lasma (power 40–70 and 500–1000 W) at temperatures of 200°C and 920°C, respectively.

The I–V characteristics for the test structure based on microcrystalline Si are shown in Fig. 1, as curves 1 (in the dark) and 2 (under illumination). In curve 1, we can see two current humps in the I–V dependence, and can also see two respective extremes $\alpha_{max1} = 16$ and $\alpha_{max2} = 8$ in the $\alpha - V$ dependence (Fig. 2a). Here we have a limit $\alpha = 2$, and, due to classification, it corresponds to a monomolecular mechanism

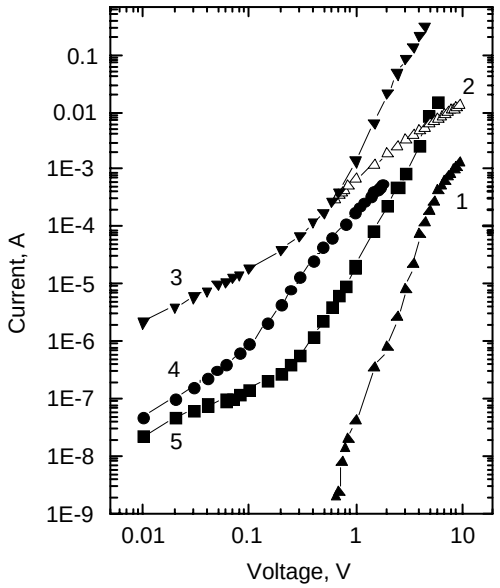

Fig. 1. I–V characteristics of solar cell test structures based on (i) microcrystalline Si—curve 1 (measured in dark), curve 2 (under illumination); (ii) microcrystalline SiC—curve 3 (dark); (iii) porous Si with a microrelief surface and an n^+–p junction—curve 4 (dark); (iv) porous Si—curve 5.

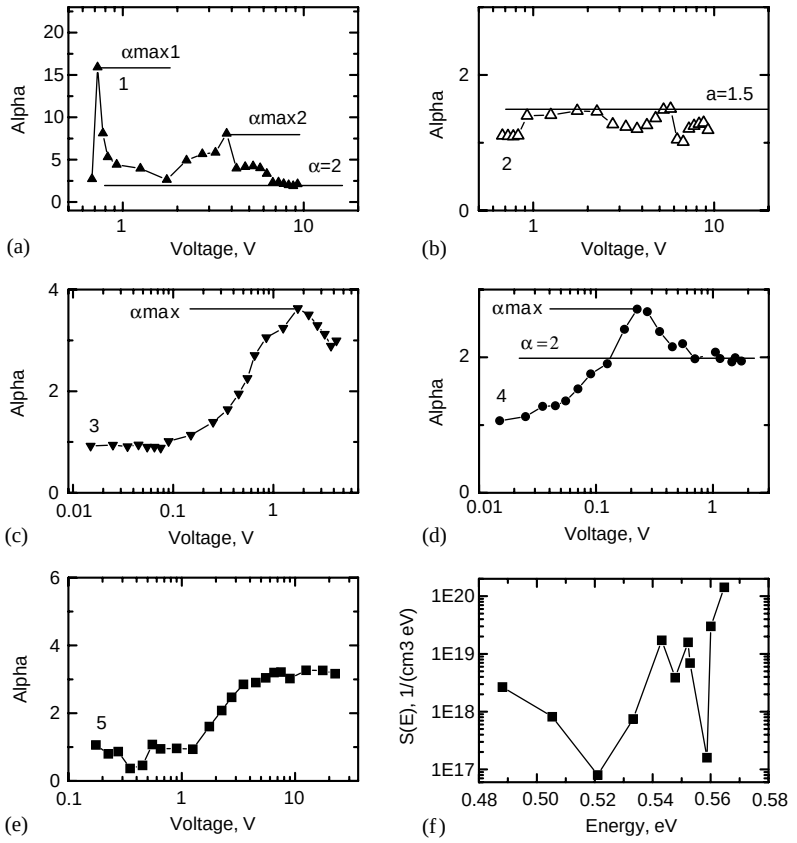

Fig. 2. $\alpha - V$ dependences (a–e) obtained from I–V characteristics corresponding to curves 1–5 of Fig. 1, and the local density of states distribution (f) corresponding to curve 5 of Fig. 1.

of recombination (approximation 9 of Table 1). Under illumination ($2000\,1\times$), in the case of a high enough photosensitivity, we have $\alpha = 1.5$ (Fig. 2b) and a bimolecular mechanism of recombination (approximation 5 of Table 1). However, when the contact restricts the current at high bias, we have a regime of low injection $\alpha < 1.5$ (approximation 4 of Table 1).

The I–V characteristic for the test structure based on a-SiC is shown in curve 3 of Fig. 1. In this case we have a high photosensitivity $S_{\mathrm{ill}}/S_{\mathrm{dark}} = 10^3$ in the range of energies $h\nu = 1-3\,\mathrm{eV}$, electron concentrations of 10^{16}–$10^{17}\,\mathrm{cm}^{-3}$ and a carrier mobility of $100\,\mathrm{cm}^2\,\mathrm{V}^{-1}\,\mathrm{s}^{-1}$ at room temperature. The I–V plot has a usual slope with a relevant extremum $\alpha_{\max} = 3.8$ in the $\alpha - V$ dependence (Fig. 2c). It corresponds to the considerable injection regime (regime 10 of Table 1).

The test structures based on porous-Si layers with a microrelief surface and an n^+–p junction were fabricated by means of three different technologies: chemical anisotropic etching, anodizing and ion implantation. Si substrates were used, with a

p-type (B-doped) resistivity of 10 Ω cm, a ⟨100⟩ orientation, and a base area of 300 μm. Chemical etching was performed in 2–10% KOH solutions at temperatures of 60–80°C. The anodizing was performed by electrochemical treatment in ethanol or aqueous HF solutions at current densities of 10–20 mA/cm^2. Ions ^{31}P were implanted at an energy of 50 keV, and a dose of 100 μC ($\sim 6 \times 10^{14}$ cm^{-2}). Post-implantation annealing was carried out at a temperature of 1000°C for 30 s. The proper porous Si layers were obtained by electrochemical processing in fluoride acid water solutions for 10–20 min.

The measured I–V characteristic (under forward bias) is shown in curve 4 of Fig. 1, and its $\alpha - V$ slope is presented in Fig. 2d. The dark curve has two exponential regions with an ideality factor of 2 at low applied fields and near 4 at high-applied fields. The last case corresponds to the regime of tunneling. At high fields, the recombination mechanism is a monomolecular one that is confirmed by a limit of

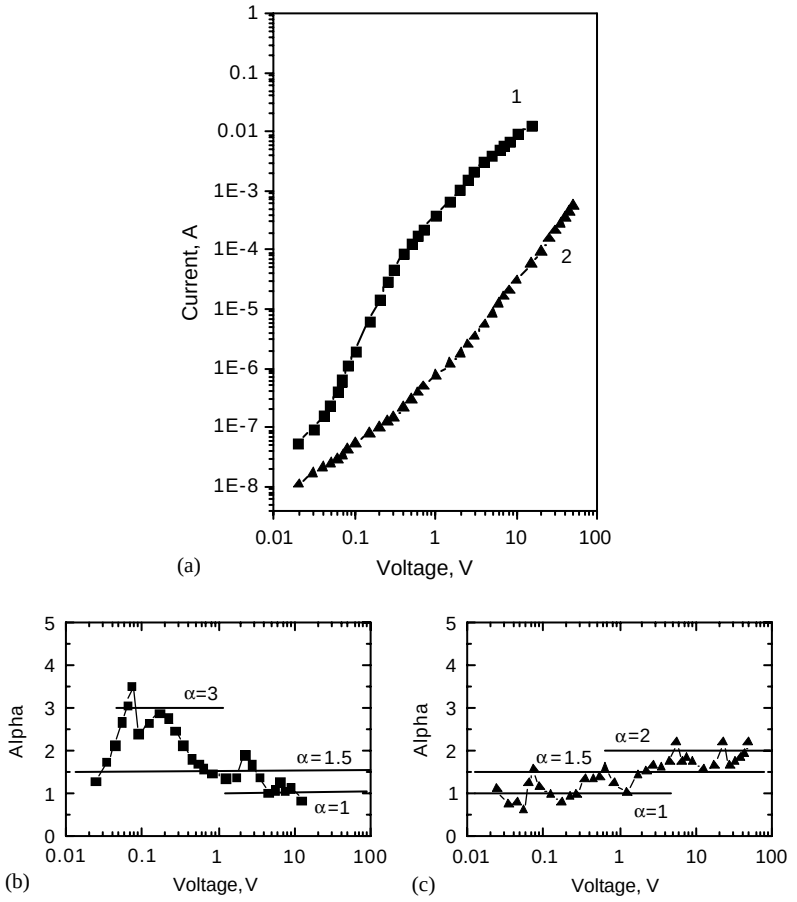

Fig. 3. I–V characteristics for the Al-porous Si–Si–Al structure, measured in the dark (a): curve 1—in forward bias, curve 2—in reverse bias; and their $\alpha - V$ dependences: (b) forward and (c) reverse.

dark and by a light slope of the I–V characteristic with $\alpha = 2$ on the $\alpha - V$ plot (Fig. 2d). The resistivity of the Si substrate is high enough, and its effect can be seen even at a voltage of 0.4 V. The minority carrier lifetime determined from the I–V characteristic was approximately 10^{-6} s, and the minority carrier diffusion length was 7×10^{-3} cm.

Curve 5 of Fig. 1 shows the dark I–V characteristic for the In-porous Si–In structure, and Fig. 2e represents its $\alpha - V$ slope. Fig. 2f shows the distribution of the local density of states $S(E)$ in the forbidden gap, as obtained using Eq. (13).

Figs. 3 and 4 represent the forward and reverse $I - V$ characteristics for the Al-porous Si–Si–Al structure with a contact area of 0.02 cm^2. The forward $I - V$ characteristics (measured in the dark—curve 1 of Fig. 3, and under illumination—curve 3 of Fig. 4) have an exponential dependence at low bias, followed by a jump in the current. The results of differential processing of these curves according to

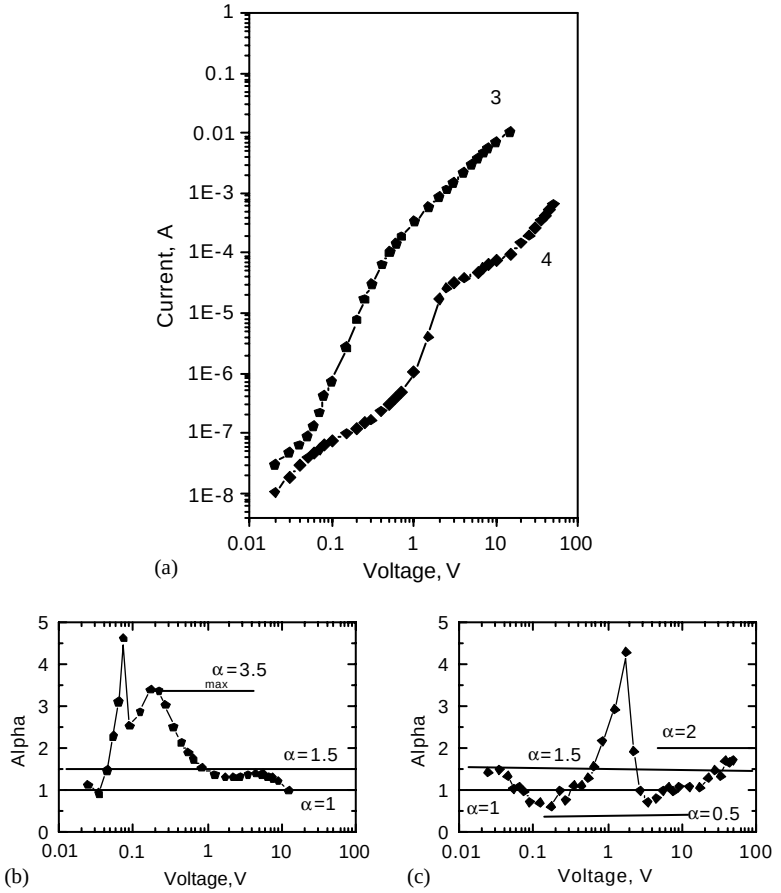

Fig. 4. I–V characteristics for the Al-porous Si–Si–Al structure, measured under illumination (a): curve 3—in forward bias, curve 4—in reverse bias; and their $\alpha - V$ dependences: (b) forward and (c) reverse.

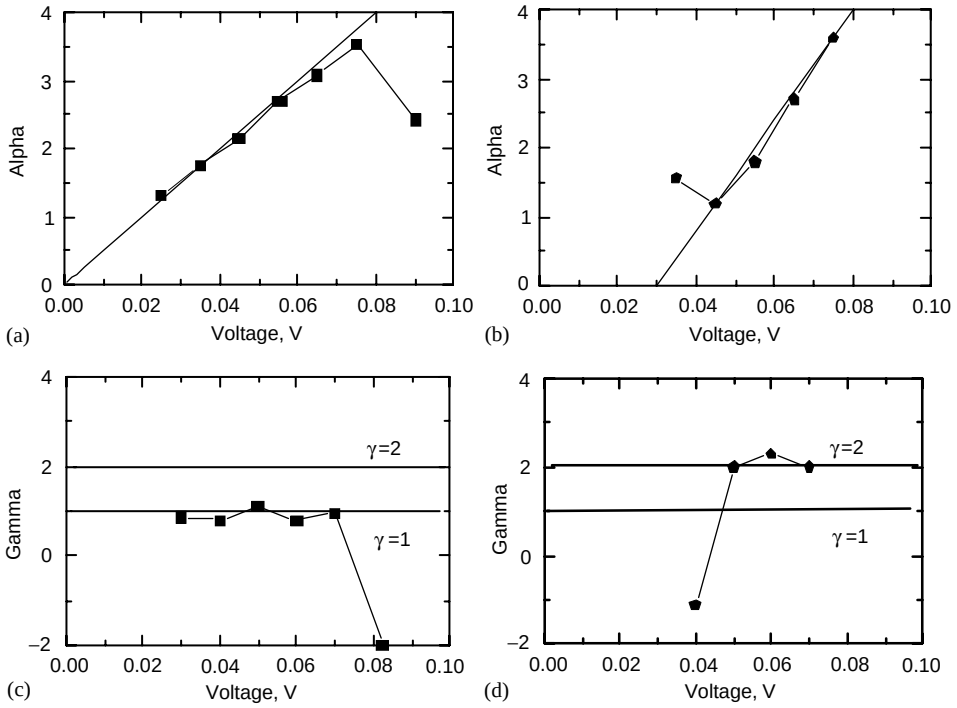

Fig. 5. $\alpha-V$ (a, b) and $\gamma-V$ (c, d) dependences corresponding to curves 1 and 3 of Figs. 3 and 4, respectively.

approximation (8) in Table 1 are presented in Figs. 3b and 4b. We see the regions with $\alpha_1 = 3$, $\alpha_2 = 1.5$ and $\alpha_3 = 1$. The illuminated $I-V$ plot has an extended region with $\alpha = 1.5$ that corresponds to bimolecular recombination.

The results of differential treatment of the $I-V$ curves at low bias, according to approximations (14) and (15) of Table 1, are presented in Fig. 5. One can see that if the dark characteristic has no cut-off in the $\alpha-V$ plot, the illuminated characteristic has it. Moreover, if the dark plot has $\gamma = 1$, the illuminated plot has $\gamma = 2$. In this way, it becomes possible to control the changes of the charge flow mechanism.

4. Conclusions

Our consideration of the charge carrier injection and recombination processes in test solar cell structures has shown that:

1. There are various charge carrier injection regimes which can characterize recombination processes in the PV semiconductor structures, according to the classification in Table 1.

2. Ultimate analysis of injection regimes allows one to determine such important physical parameters of test structures as the lifetimes of the minority carriers, the distribution of the localised density of states, the electron or hole capture coefficients in the localised states, etc.
3. Differential processing of the I–V curves allows one to obtain the fine structure of the current, and to recognize the small differences in characteristics with respect to voltage.
4. The power-law and exponential behavior of the I–V curves can be determined by the differential technique: the α value gives a power law, the γ value gives an exponential law.
5. In typical Si solar cell structures, recombination has a monomolecular mechanism for the dark I–V curves with $\alpha = 2$. It is a bimolecular one for the illuminated I–V curves, with $\alpha = 1.5$.
6. Additional differential processing of the I–V curves by Eq. (13) allows one to distinguish the distribution of the local density of states in the forbidden gap of the semiconductor structure.

These peculiarities are important, and can be used in practice for the study and characterization of various solar cell structures, in parallel with other well-established direct characterization techniques: the spectral response, lifetime measurements, LBIC, SVP, etc.

Acknowledgements

This work was supported partially by the NATO Science for Peace project # 97-1829, and by the Ukrainian Ministry of Education and Science and STCU project #1556.

References

[1] F. Stockman, in: Halbleiterprobleme, Vol. 6, Viervag, Braunschweig, 1961, p. 279.
[2] M. Lampert, P. Mark, Current Injection in Solids, Academic Press, New York and London, 1970.
[3] R. Baron, J.W. Mayer, Double injection in semiconductors, in: R.K. Willardson, A.C. Beer (Eds.), Semiconductors and Semimetals, Vol. 6, Academic Press, New York and London, 1970, p. 201.
[4] V.I. Strikha, Theoretical Fundamentals of Metal–Semiconductor Contact, Naukova dumka, Kyiv, 1974.
[5] B. Pellegrini, Adetailed analysis of the metal–semiconductor contact, Solid-State Electon. 17 (1974) 217–237.
[6] P.M. Karageorgi-Alkalaev, A.Yu. Leyderman, A.I. Adirovih, Currents of Double Injection in Semiconductors, Soviet Radio, Moscow, 1978.
[7] E.H. Roderick, Metal–Semiconductor Contacts, Claredon Press, Oxford, 1978.
[8] S. Nespurek, J. Sworacowski, Phys. Status Solidi A 49 (1978) K149.
[9] A.N. Zyuganov, S.V. Svechnikov, Contact-Injection Phenomena in Semiconductors, Naukova dumka, Kyiv, 1981.

[10] G.D. Bagratishvili, R.B. Dzhanelidze, D.A. Jishiashvili, A.N. Zyuganov, V.M. Mikhelashvili, I.V. Piskanovskii, P.S. Smertenko, Phys. Status Solidi A 65 (1981) 701.
[11] A.N. Zyuganov, Yu.G. Pismennyi, S.V. Svechnikov, P.S. Smertenko, Phys. Status Solidi A 45 (1978) 631.
[12] J.C. Pfister, Phys. Status Solidi A 24 (1974) K15.
[13] C. Manfredotti, C. De Beasi, S. Galassini, G. Micocci, L. Ruggiero, A. Tepore, Phys. Status Solidi A 36 (1976) 569.
[14] P.S. Smertenko, et al., USSR Patent # 4617198, 1989.
[15] N.M. Volodin, P.S. Smertenko, L.L. Fedorenko, A.V. Khanova, Semiconductors 32 (12) (1998) 1273–1277.
[16] A.N. Zyuganov, M.Yu. Gusev, T.V. Torchinskaya, Ukr. Phys. J. 35 (1990) 1241.
[17] S.V. Svechnikov, P.S. Smertenko, A.V. Smirnov, I.O. Spychak, Ukr. Phys. J. 43 (1998) 234.
[18] T.Ya. Gorbach, P.S. Smertenko, S.V. Svechnilov, M. Kuzma, G. Wish, R. Ciach, Appl. Surf. Sci. 154–155 (2000) 495.
[19] A.N. Shmyryeva, V.A. Kochelap, V.V. Naumov, P.S. Smertenko, Proceedings of the 17th European PV Solar Energy Conference and Exhibition, Munich, Germany, 2001.